Ultrasonics and electromagnetics for a wireless corrosion sensing system embedded in structural concrete

K. Hietpas[†], B. Ervin[‡], J. Banasiak[†], D. Pointer[‡†], D. A. Kuchma[‡‡],
H. Reis[‡] and J. T. Bernhard[†]

University of Illinois at Urbana-Champaign, Urbana, IL 61801, USA

Abstract.   This work describes ongoing development of an embedded sensor system for the early detection and prevention of deterioration of reinforcing steel tendons within reinforced concrete. These devices will evaluate the condition of the steel tendon using ultrasonic techniques and then wirelessly transmit this data to the outside world without human intervention. The ultrasonic transducers and the interpretation of the sensed signals that allow detection and prognosis of tendon condition are detailed. Electrical characterization of concrete mixtures used in bridge construction is conducted and a wideband microstrip antenna is designed and fabricated to operate between 2.4 and 2.5 GHz when embedded in such a medium. Simulations and measurements of the embedded antenna element are presented. Transceiver selection and implementation are discussed as well as future work in operational protocols, sensor networking, and power sources. By implementing commercially available off-the-shelf components whenever possible, these devices have the potential to save millions of dollars a year in evaluation, repair and replacement of reinforced concrete.

Keywords: ultrasonic guided waves; structural concrete; corrosion; embedded wireless sensors; embedded antenna.

1. Introduction

Highway systems are aging and slowly deteriorating, causing upkeep and replacement costs to continuously increase. This deterioration is caused primarily by corrosion occurring on the reinforcing steel tendons (rebar) used in these concrete structures. Assessment of the condition of these tendons is a difficult task, considering the steel is usually buried beneath 8 or more centimeters of concrete. There are no definitive empirical methods for detection of deterioration. Therefore repairs and replacements are based on mainly visual indications of failure. The cost of inspecting, rehabilitating and replacing degraded pieces of structures in the United States alone, using the current methodology, is estimated to be near $210 billion dollars (Fuhr, *et al.* 1995). With proper testing methods that require fewer visual inspections and provide more accurate information about the condition of the steel reinforcement, this expense could be drastically reduced.

[†]Electromagnetics Laboratory, Department of Electrical and Computer Engineering
[‡]Non-destructive Testing and Evaluation Laboratory, Department of General Engineering
[‡†]National Center for Supercomputing Applications (NCSA)
[‡‡]Department of Civil and Environmental Engineering

Current and proposed methods of evaluating the degree of steel tendon degradation can be imprecise and do not provide an accurate representation of what is occurring within the concrete. Visual tests are comprised of observing cracks in the girders and rust occurring on the outside of the concrete. The degradation has then progressed so far that a majority of the structure needs to be replaced. Other evaluation methods range from ground penetrating radar (GPR) to dragging a chain on bridge decks and listening for echo discrepancies in order to characterize the interior of these concrete structures (Turner 1994, Rhim 2000 and Sinha 2003). Pinpointing positions of decay with ground penetrating radar is problematic due to several practical considerations, such as multi-level interference and the lack of a definitive method for interpretation of decay extent.

Some proposed methods involve embedding devices into concrete in order to perform tests within the structures and transmit information to the outside world (Ross 2003, Watters 2002, Carkhuff 2003). The devices relay information about the corrosion factors (usually chloride ion concentration) within the concrete. These devices, however, are completely passive until a reading unit is placed near them, still requiring human interaction to obtain any data. Another method (e.g. Fuhr, *et al.* 1998) involves embedding long sections of fiber optic cables into roadway and bridge structures to test for similar parameters. Fiber optics, however, must be placed within the entire structure and allowed an outlet from the concrete. These devices are designed to test for the proper conditions for corrosion to occur but do not actually test for corrosion damage. Therefore, they may report excessive levels of chloride ions or extreme temperatures whether or not the tendons are still healthy.

The purpose of the present project is to create a system of wireless embedded sensors that utilize ultrasonic techniques to test the condition of reinforcing tendons in concrete. For example, prestressed concrete bridge girders are constructed in dedicated factories that have stringent control over the process. The steel tendons are held under tension while the concrete is formed around them. The tendons are cut, causing the girders to bow; bowing counteracts the weight of the fully formed bridge that these girders support. A cross section of a bridge girder is shown in Fig. 1a. The devices will be mounted directly to the steel tendons as shown in Fig. 1b. These will interact in a large network to characterize and locate any corrosion damage in the reinforcing steel. The information

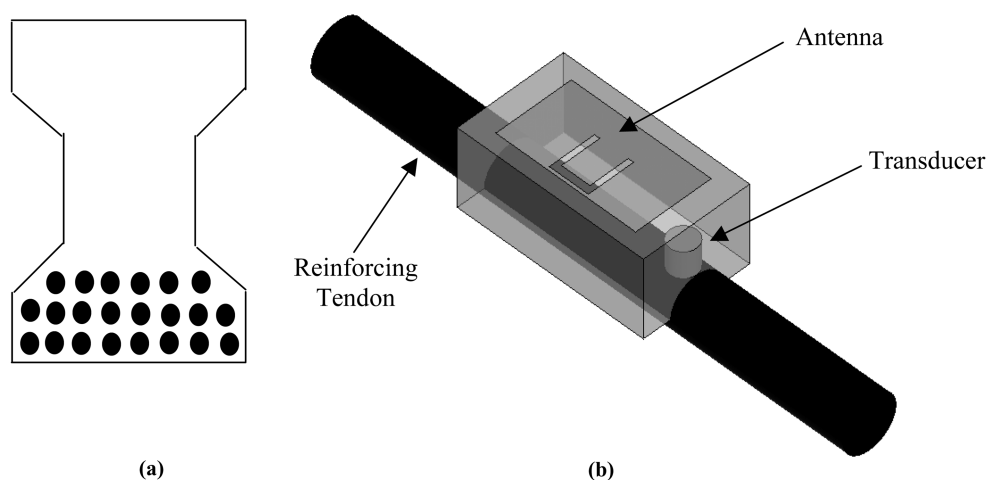(a)   (b)

Fig. 1 Cross section of pre-stressed girder with approximate positions of reinforcing tendons shown (not to scale) (a) and proposed sensor implementation mounted to reinforcing tendon (b)

gathered from the sensors will be relayed to an independent base station situated on the exterior of the bridge, which will upload that information via the commercial cellular network to the department of transportation.

Creation of these devices necessarily requires input from an interdisciplinary team. In the following two sections, we discuss two important aspects of this system: the active ultrasonic techniques used to sense the tendon condition and the electromagnetic design that enables wireless communication of this data from within the girder itself.

2. Ultrasonic sensing and data interpretation

The mechanics of corrosion in reinforced concrete leads to an expansive product (rust at the cathode) and a loss of steel reinforcement diameter (at the anode) (Carino 1999, Reis 2003). These reactions degrade the strength and aesthetics of the concrete structure due to disruption of the bond at the interface between the steel and the surrounding concrete, loss of steel cross-sectional area, and longitudinal cracking in the concrete with rust stains. Fig. 2 illustrates the progressive general phases of degradation in reinforced concrete due to corrosion.

Currently, there are several techniques being developed to assess the degradation of concrete structures due to corrosion (Reis and Ervin 2003). Among these, the use of guided ultrasonic waves has been proposed as a methodology for detecting and evaluating structural degradation caused by the corrosion process. Many sources provide a good analytical review of ultrasonic waves in cylindrical waveguides (Redwood 1960, Kolsky 1963, Rose 1999, and Pavlakovic 2001). Guided ultrasonic waves have also been used to detect simulated corrosion degradation in reinforced concrete specimens including small notch defects (Pavlakovic 1999) and debonding (Na 2002, Wu 2001, Wang 2001). Rose, *et al.* (2002) have also discussed the importance of using ultrasonic guided waves for inspection in industrial processes.

Guided waves are combinations of longitudinal and shear waves that continually interact with the boundaries to form a composite wave (Rose 2002). Energy flows mainly along the direction of the guiding configuration (Auld 1973). If the geometry of the waveguide affects the flow of energy, then the speed and attenuation of the waveform that has propagated through the waveguide should give a strong indication of its geometry. For example, Chung (1978) measured the change in the speed of a transmitted ultrasonic pulse for different diameters of concrete embedded reinforcement. His findings confirmed that the geometry could be determined from the group velocity of guided ultrasonic waves. For the current investigation, guided ultrasonic waves will be used to assess simulated corrosion damage in the form of debonding between the embedded steel and the surrounding mortar.
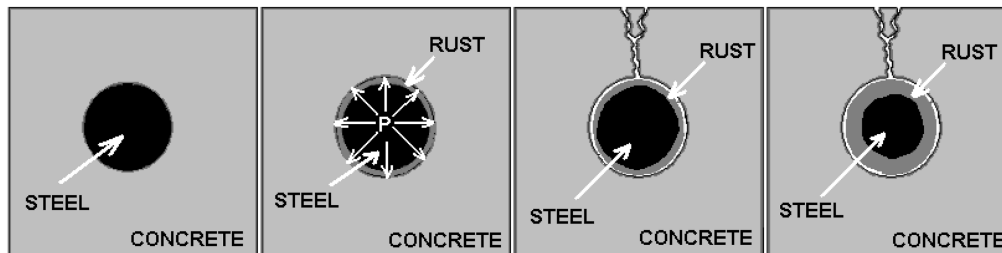

Fig. 2 Progressive phases of corrosion degradation in reinforced concrete

Tape

25% Debonded
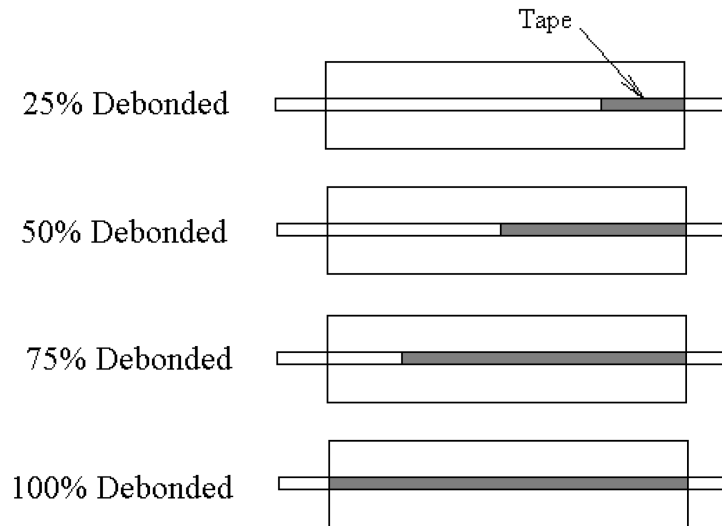
50% Debonded

75% Debonded

100% Debonded

Fig. 3 Schematic diagram showing four test specimens with increasing amounts of tape-simulated debonding

Specimens were manufactured to simulate the entire range of possible delamination to estimate the feasibility of the technique in detecting corrosion damage. To simulate bond loss at the interface between the steel tendon and the surrounding concrete, a range of different lengths of tape were wrapped around the steel reinforcing bars (bar size #4) to inhibit bond during hydration of the surrounding mortar (0.45 water to cement ratio). The reinforcing steel bars, with 106.68 cm (42") in length, were centered within the surrounding mortar specimens, which had the dimensions 10.16 cm × 10.16 cm × 91.44 cm (4" × 4" × 36"). Twelve specimens were manufactured, with the length of the tape starting at 7.62 cm (3") and ending at 91.44 cm (36") (completely debonded) in 7.62 cm (3") increments. The tape started on each specimen at the end where the sending transducer was mounted. Fig. 3 provides an illustration of the test specimens. The tape was used to assess if the development of a layer of dissimilar material would impact the attenuation of the signal. This was considered to better simulate debonding due to corrosion as opposed to pitting corrosion. In subsequent testing, accelerated corrosion methods are being used.

A broad range of frequencies was evaluated to test the specimens. A lower frequency range was used for final testing to avoid high attenuation of the waveform. However, Pavlakovic, *et al.* (1999) found that higher frequency testing bands may attenuate less due to lower amounts of energy leakage to the surrounding concrete because of the wave structure of the generated higher guided wave mode. The specimens were tested with direct (parallel to the tendon to generate mainly longitudinal wave modes) and indirect (perpendicular to the tendon to also generate flexural modes) transducer arrangements using the equipment setup shown in Fig. 4. In the first experiment, a frequency of 200 kHz, with a tone burst of 5 square pulses was used to excite the sending transducer. The pulse had a peak-to-peak voltage of 200 V, and the indirect transducer configuration was used to generated flexural modes. Note that since the transducers draw very little current (less than 0.2 mA for a 200 V signal over 200 tone bursts at 80 kHz, for example), the upper level of power required for one set of measured to be on the order of 30 mW, which is quite feasible in a small portable electronic package. The filter had a high pass setting of 50 kHz and a low pass setting of 250 kHz. Four signals were captured for each specimen and used
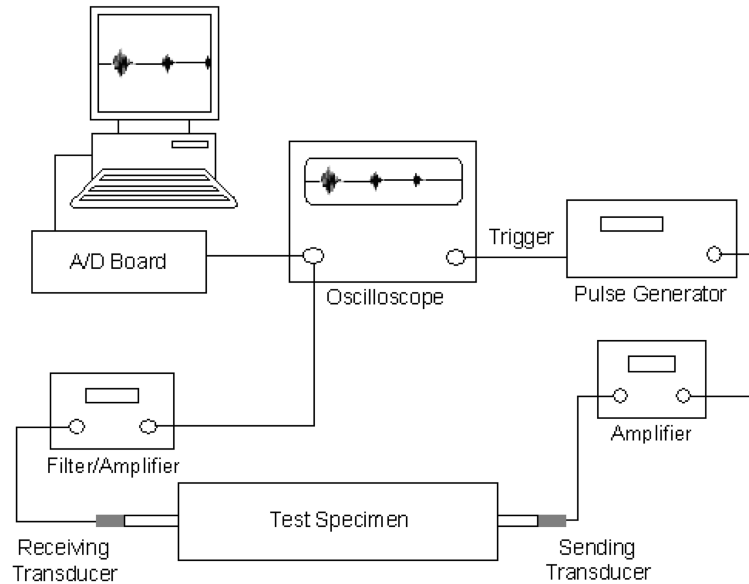
Fig. 4 Schematic diagram of laboratory testing setup showing the transducers mounted in direct transmission
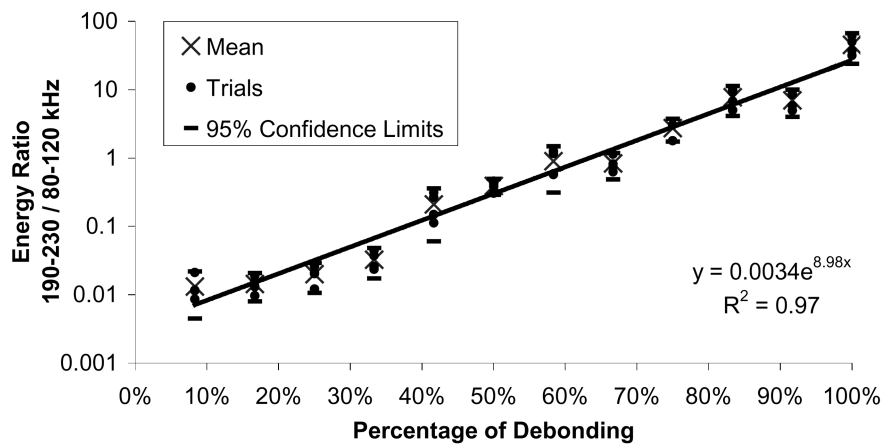

Fig. 5 Ratio of signal energy for two frequency bands vs. percent of debonding using indirect transducer arrangement

for averaging the waveform corresponding to the first flexural mode. To avoid transducer coupling issues that may cause variation between specimens, an energy ratio from two frequency bands within the same spectral density curve was used, i.e., the energy within 190 to 230 kHz frequency bandwidth was divided by the energy within 80 to 120 kHz. Fig. 5 shows the plot of the energy ratio for the first flexural wave mode. A high coefficient of determination (R^2=0.97) was obtained.

In a second experiment, a tone burst of 15 rectangular pulses with a pulse width of 3.33 µs was used to excite the sending transducer. The pulse had a peak-to-peak voltage of 200 V. The filter was set with a high pass frequency of 50 kHz and a low pass frequency of 300 kHz, with a gain of 40 dB. Fig. 6 shows the area under the power spectral density curve versus the percent of debonding, using a direct
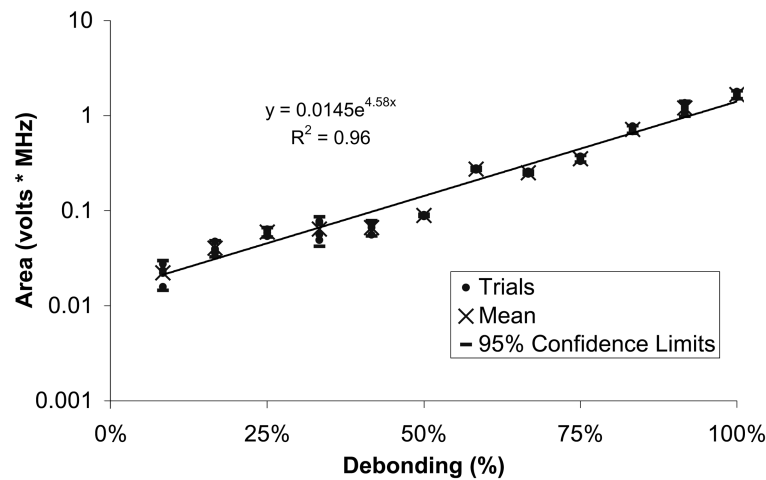
Fig. 6 Area under the power spectral density curve vs. percent of debonding using a direct transducer arrangement

transducer arrangement for the frequency band of 100 kHz to 200 kHz.

The coefficient of determination for the exponential trend line is 0.96. Fig. 6 indicates that less energy leaks into the surrounding mortar as more debonding occurs. Similar results were obtained for an indirect transducer arrangement. Fig. 6 shows that change in the area under the power spectral density curve can also be used to detect and estimate the amount of delamination between the steel tendon and surrounding mortar.

It should be noted that in actual bridge girders, one may encounter varying levels of dynamic traffic that induce strain in the reinforcing tendons that may also generate a signal that could be received by the ultrasonic transducers. The use of signal filtering will filter out environmental and other noise. Alternatively, the long-term monitoring system can be used to collect data during periods where there is little to no traffic where the impact of dynamic traffic induced strain will be minimal or non-existent.

Active ultrasonic transducers will be integrated into the final package that will be embedded into concrete girders. The final package will also include the radio and antenna necessary for wireless communication of the sensed data. The design of these components is discussed in the next section.

3. Electromagnetic design for wireless communication

3.1. Frequency selection

Two different frequency bands were considered for the operation of the wireless communication link for this system. The FCC allocates several different bands for the general use of Industry, Science and Medicine (ISM). These bands do not require special permits and only require that systems not interfere with each other. Two ISM bands, 2.4 to 2.5 GHz and 5.725 to 5.85 GHZ, were considered due to the available bandwidth for data communication and the relatively small antenna size that would be required. The 2.4-2.5 GHz frequency band was chosen for this system due to the availability of off-the-shelf radio components.

3.2. Electrical characteristics of concrete

The electrical properties of the concrete used in girder construction were investigated to enable accurate modeling and design of the antenna that will be embedded in the structure. Two different mixtures of concrete were tested for their relative permittivity, permeability, and conductivity from 1 GHz to 3 GHz. These mixes, currently used in the construction of highway bridges, are detailed in Table 1.

Others have characterized the electrical properties of various concrete mixtures over frequency (e.g. Rhim, *et al.* 1998). Rhim, *et al.* (1998) tested various samples of concrete over a large frequency range including 1 to 20 GHz. Near 2.4 GHz, he reports that the relative permittivity was approximately 4 while the conductivity was close to zero. To confirm this information for our particular mixes, samples of concrete were fabricated and measured. Samples were cast and allowed to air-dry for a minimum of seven days. All the samples were formed into cylinders with diameters of 7.62 cm (3"), 10.16 cm (4"), and 15.24 cm (6"). Each contained a slot to accommodate the dielectric probe that was used to measure the electrical properties of the concrete samples.

The Hewlett Packard 8507A Dielectric probe was used in conjunction with an Agilent 8510C Network Analyzer. Using this probe, the electrical properties of the various size and sand content samples were gathered. The findings of these tests are comparable to Rhim, *et al.*'s findings (Rhim, *et al.* 1998); the average relative permittivity of Mix #1 was approximately 4 while the conductivity varied between 0 and 0.04 Siemens/m. The permittivity and conductivity of Mix #2 were noticeably higher than the previous findings, having a relative permittivity of approximately 7 and conductivity near 0.1 Siemens/m. This result is most likely due to the higher proportions of cement and water in Mix #2.

The amount of expected signal loss within concrete at this frequency is found using Eqs. (1)-(3) (Ramo, *et al.* 1994). In Eq. (1), γ is the complex wave propagation coefficient; α the attenuation coefficient; β, the wave vector number; ω, the angular frequency (equal to $2\pi f$, where f is the operating frequency); μ, the permeability; ε, the permittivity; and σ, the conductivity. These calculations indicate that the attenuation of a signal within concrete will be very low. In 10 cm (approx. 4 inches) of concrete, a signal will only lose approximately 2.11 dB in Mix #1 concrete and 6.49 dB in Mix #2 at an operating frequency, f, of 2.448 GHz.

$$\gamma = \alpha + j\beta = \frac{\sigma}{2}\sqrt{\frac{\mu}{\varepsilon}} + j\omega\sqrt{\mu\varepsilon} \tag{1}$$

Table 1 Content of measured concrete mixtures

Constituent	Type	Mix #1 (lbs/ft^3)	Mix #2
Cement	Type I Portland Cement	22.41	36.30
Fine Aggregate	River Sand	41.85	32.94
Coarse Aggregate	Trap Rock (3/4")	67.41	66.41
Water	Tap Water	9.85	11.59
Silica Fume	Force 10,000 (Grace)	10.25	7.26
Superplasticizer	ADVA Flow (Grace)	0.186	0.607
Accelerator	CaCl2	0.014	0.037

$$\alpha = \frac{\sigma}{2}\sqrt{\frac{\mu}{\varepsilon}}\left[\frac{Np}{m}\right]$$ (2)

$$Loss[dB] = \alpha \left[\frac{Np}{m}\right] \times 0.1[m] \times 8.656\left[\frac{dB}{Np}\right]$$ (3)

3.3. Antenna selection, design, and simulation

A microstrip antenna design was chosen for this application, since the rugged planar design lends itself well to integration with the rest of the embedded package and will not disturb the structural integrity of the concrete girder. Unfortunately, a standard microstrip patch has a very narrow bandwidth (~2%) (Howell 1975), which makes it unsuitable for operation in the chosen frequency band. Thus, a microstrip U-slot antenna was selected because it possesses a far greater operational bandwidth (~10%) than a standard patch antenna (Huynh 1995). Using the design methodology described by Weigand, *et al.* (2003), a U-slot microstrip antenna was specified to operate between 2.4 and 2.5 GHz when embedded in concrete. The U-slot antenna was designed on a substrate with permittivity of 2.2 and thickness of 3.175 mm. A diagram of the antenna with dimensions is provided in Fig. 7.

The Weigand method of designing a U-slot antenna allows for placement of the resonance points -- points where the imaginary component of the antenna's input impedance is zero. After designing the resonance points of the antenna using Weigand's method, the antenna design was further optimized using a commercial electromagnetic computational package (IE3D®, Zeland 1999) to be impedance matched at the appropriate frequencies when embedded. Another simulation package, Ansoft HFSS® (2002), was also used to evaluate the design and compare results before the design was fabricated. Fig. 8 provides a comparison of the simulated return loss (S_{11}) obtained from the two simulation packages when the antenna is simulated below 5 cm of concrete. This data indicates that the antenna exhibits an acceptable impedance match (with $|S_{11}|$ less than –9.54 dB and VSWR (voltage standing wave ratio) below 2:1) in the 2.4-2.5 GHz frequency band when it is embedded in concrete. Radiation patterns of the embedded antenna are discussed in the next section.
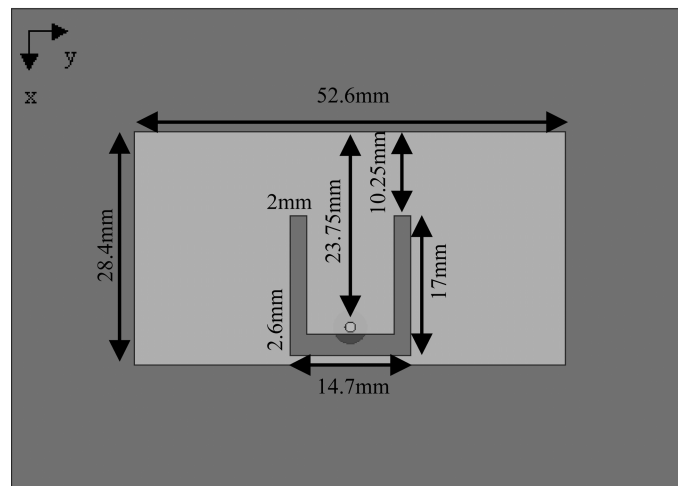

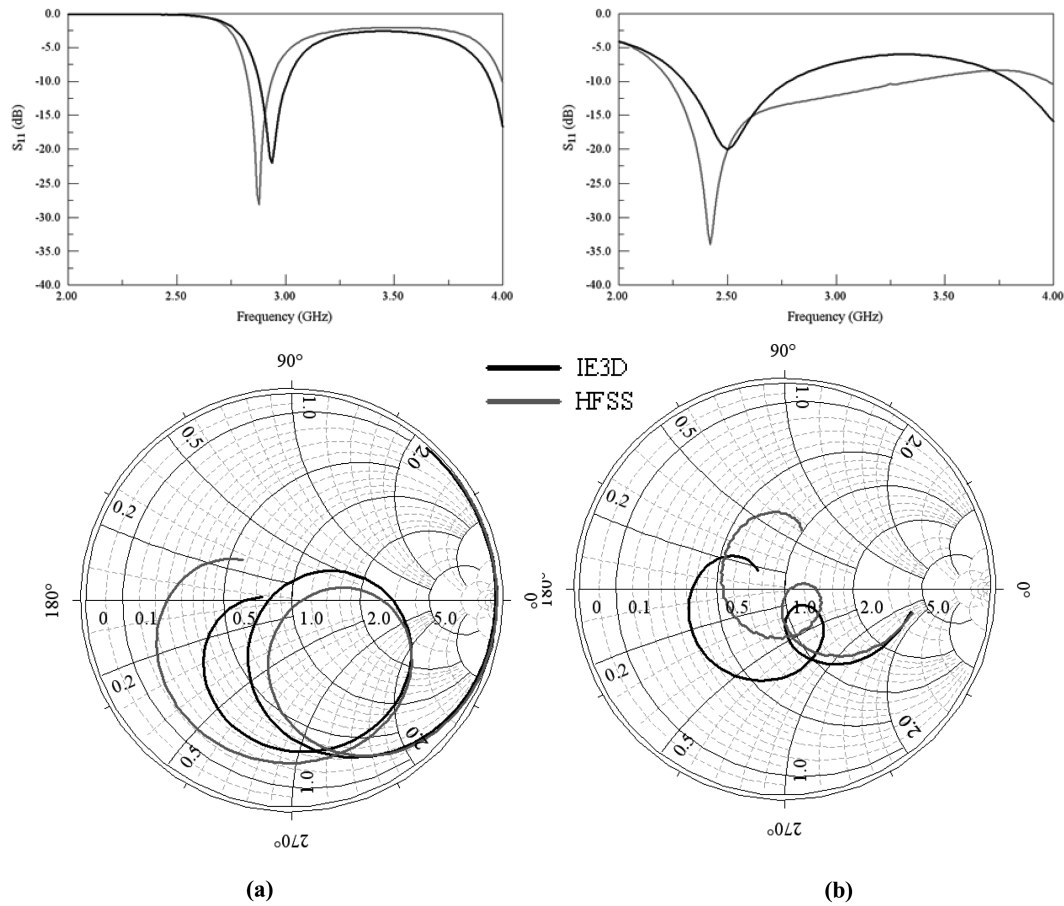Fig. 7 Diagram of U-slot antenna with dimensions shown

Fig. 8 Simulated return loss (S_{11}) and impedances in air (a) and concrete (b)

3.4. Antenna fabrication, testing and results

After verifying that the antenna would present an impedance match within the required frequency band, a prototype was fabricated. Using Rogers Duroid® 5880 as the substrate material, the antenna shown in Fig. 9a was created along with a choke and cable long enough to extend out of a concrete block as shown in Fig. 9b. The choke ensures that the long metallic cable attached to the antenna does not radiate and distort the pattern of the antenna element. The return loss (S_{11}) and radiation patterns of this assembly were tested before being embedded into the concrete specimen. Measurements in air agreed very closely with the simulations and are not included here for brevity. In air, the antenna exhibits a uniform radiation pattern that is consistent with a microstrip patch antenna (Howell 1975).

The antenna assembly was then coated with a spray-on plastic coating to electrically isolate it from the concrete. Next, the antenna was encased in a sample of Mix #1 concrete measuring 20.32 cm × 20.32 cm × 30.48 cm (8" × 8" × 12"). The antenna was embedded halfway into the block so that it was about 10 cm away from the concrete face. This distance was judged comparable to the space between the bottom tendons and the face of the concrete girder. Care was taken to maintain proper alignment and placement within the concrete specimen. A picture of the completed embedded antenna for test as
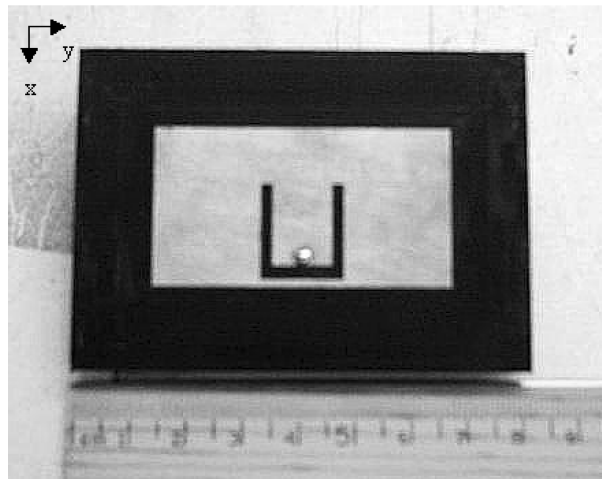
(a)
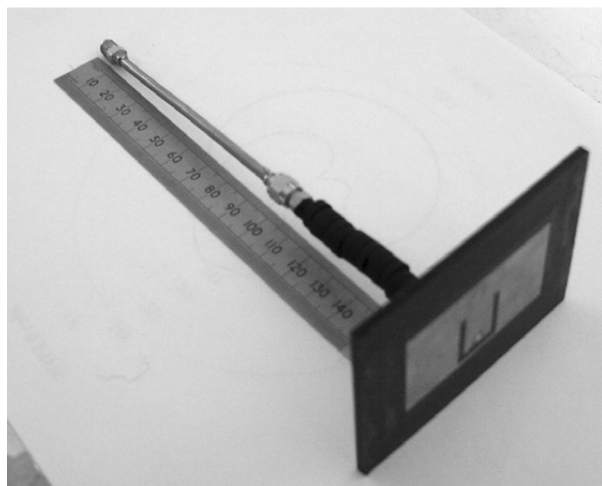
(b)

Fig. 9 U-slot antenna (a) and assembly (b)

well as a graphic of the simulated version of the embedded antenna in HFSS® are provided in Fig. 10. The cable extends far enough out of the concrete block to be connected to test equipment without inducing any mechanical stress on the cable.

The concrete block assembly was then tested with the network analyzer and the return loss and radiation patterns were measured and compared to the simulated data (Fig. 11). The operating band of the embedded assembly (defined by a return loss less than −9.54 dB) encompasses the range from 2 GHz to well above 4 GHz as shown. The measurements show a larger bandwidth than expected and the antenna operates well in the 2.4-2.5 GHz band. The increased bandwidth of the embedded prototype is most likely due to inhomogeneities (i.e. aggregate and small air pockets) in the concrete sample that were not included in the simulations. The far field radiation patterns of embedded concrete assembly were measured in an anechoic chamber. The test setup in the anechoic chamber, pictured in Fig. 12, was
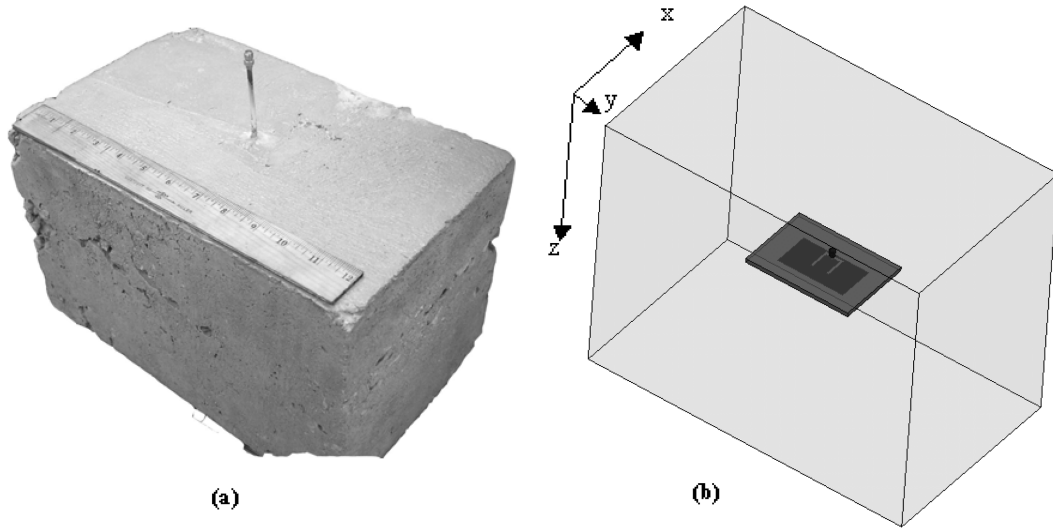
Fig. 10 Antennas embedded in concrete specimens (a) physical specimen (b) modeled in HFSS®
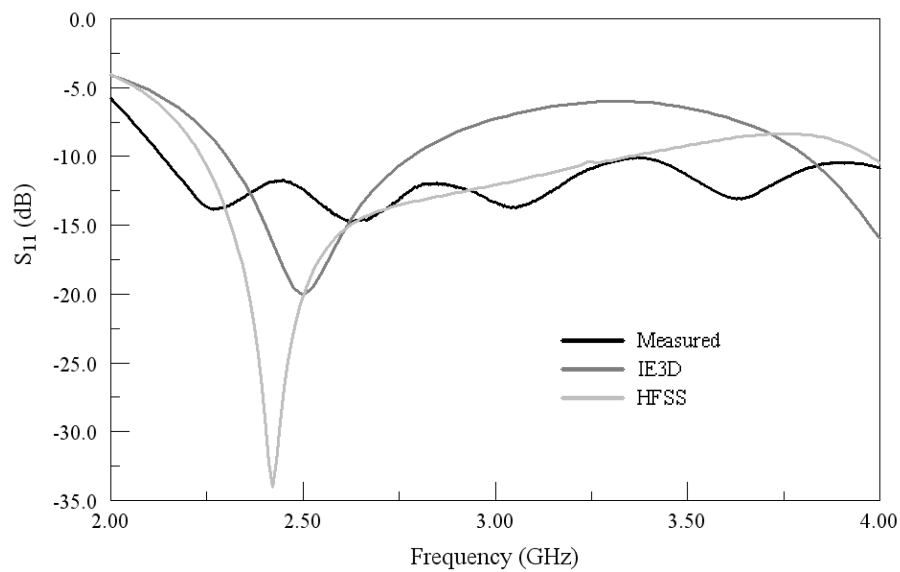

Fig. 11 Measured return loss (S_{11}) in concrete compared to simulated results

reinforced to support the weight and size of the concrete specimen. The far field patterns of the assembly are shown in Fig. 13 along with simulation results from HFSS© using a conductivity of 0.1 Siemens/m (which is slightly higher than expected for this mixture of concrete). Again, the presence of inhomogeneities in the concrete specimen can account for the difference in effective conductivities. The maximum gain from this assembly is approximately −7 dBi.

To determine the maximum possible range of the embedded assembly using an antenna with −7 dBi gain, the Friis Transmission Formula (Eq. (4)) was used (Griffiths 1987). This is the standard equation
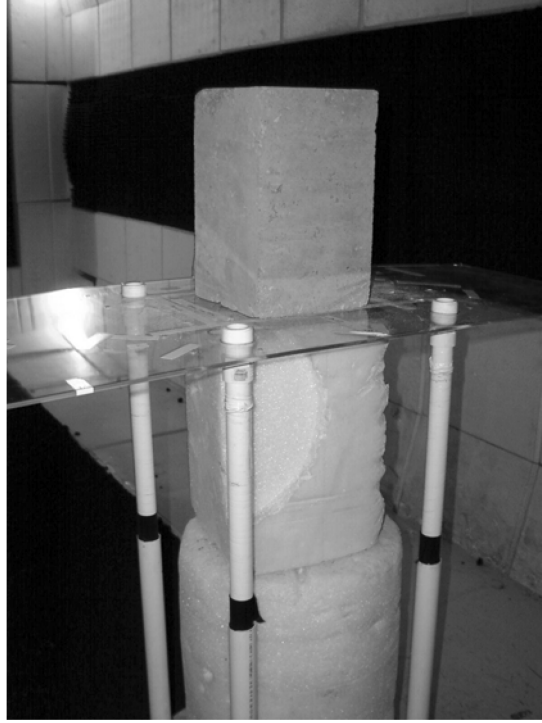
Fig. 12 Embedded assembly in concrete specimen in the anechoic chamber for radiation pattern tests

used for determining the received power in a typical line-of-sight wireless transmission. The following assumptions were made for these calculations:
- the embedded transceiver broadcasts (P_S) with 1 mW (0 dBm)
- receiver sensitivity (minimum P_L) is −80 dBm
- gain of the TX antenna (G_t) is −7 dBi
- gain of the RX antenna (G_r) is 6 dBi (typical patch antenna in air)
- mismatch factor (q_t) is 0.98 (found using the network analyzer)

The maximum range found using Eq. (4) under these conditions would be 87 meters. For most bridge applications, this range will be perfectly adequate to send a signal between the embedded transmitter and the local base station. This external base station, powered with solar cells, will then relay all information through the cellular telephone system to the State Department of Transportation.

Transmission of the signal will take place primarily through the bottom of the girder and all link budgets have used this assumption. While steel reinforcement will act as a

$$P_L = \frac{\lambda^2}{(4\pi r)^2} e_t q_t D_t e_r q_r D_r |p_r \cdot p_t|^2 P_S \tag{4}$$

$$e_t D_t = G_t \qquad e_r D_r = G_r \tag{5}$$

$$q_t = \frac{4 R_A R_S}{|Z_A + Z_S|^2} \tag{6}$$

(a)   **(b)**

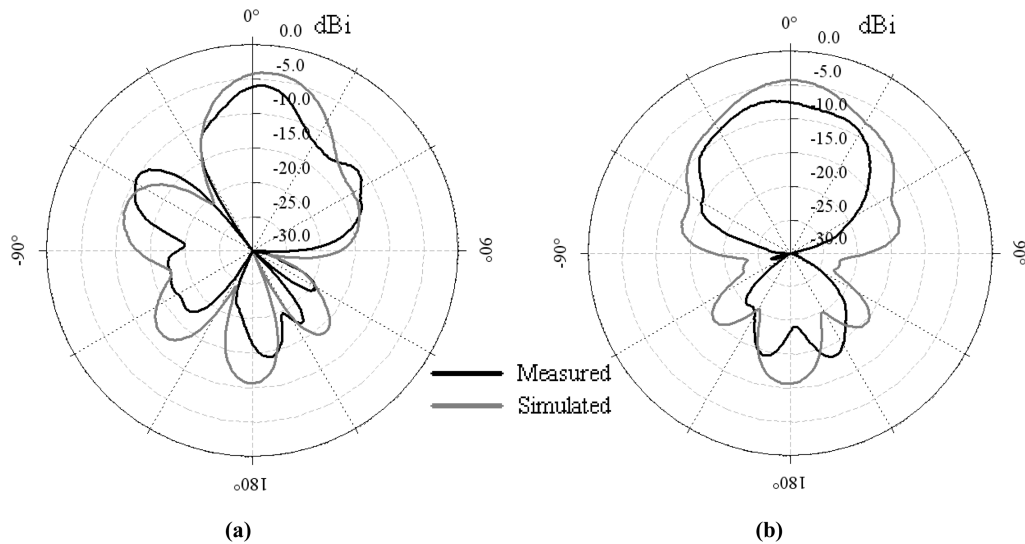Fig. 13 Measured and simulated radiation patterns in the E-plane ($\phi = 0^0$) (a) and H-plane ($\phi = 90^0$) (b) of the embedded antenna assembly in concrete.

reflector in general, these devices will primarily be located on those tendons closest to the surface of the concrete and positioned to look downward toward the bottom side of the girder. Since the antenna is a microstrip design, the presence of the ground plane between the rest of the antenna and any other reinforcing tendons insures that other tendons will have little to no affect on the transmission of the signal. We have conducted (but not included here) detailed electromagnetic simulations of the antenna inside concrete with multiple reinforcing tendons and found that there is no appreciable effect on the antenna performance with correct deployment. A girder fabrication strategy will be developed that will allow the sensors to be installed simply and correctly to insure that the system can use each sensor along the tendon without interactions from other reinforcing tendons.

3.5. Transceiver selection and power requirements

Based upon the previous choice to use the 2.4 to 2.5 GHz ISM band, a suitable transceiver was sought to allow proper control and up to 50 mW of output power. A transceiver from Maxstream (the 24XStream™ 2.4 GHz OEM RF Module) was selected that offers a suitable package size with straightforward programming capabilities. Each radio transceiver can be programmed to communicate with a specific module or modules using unique media access control (MAC) addresses. A development kit from the manufacturer enables transceiver programming as well as communication testing through a computer program. This program also contains a diagnostic tool that will repeatedly send prearranged packets back and forth between two radios to verify their operation.

The power requirements for this embedded system have been estimated using a worst case operation scenario. Assuming that the condition of the tendon is sensed once per month, the transducer uses a 200-packet pulse at 200 V with a repetition rate of 80 kHz and the radio transmitter is in sleep mode (which draws 26 μA) except for when awakened by a signal from the external base station and transmits full power when awake, the battery capacity required will be approximately 19 mA-h over a

30-day period. Most of this capacity is used by the sleep mode of the transceiver over the 30-day time frame.

To meet these power requirements, we plan to implement a piezoelectric energy harvesting scheme with rechargeable batteries that takes advantage of the ambient vibrations of the structure due to traffic or other loading. Recent work in the area of piezoelectric energy harvesting (Ottman, *et al.* 2002, Sodano, *et al.* 2003, Ottman, *et al.* 2003, Sodano, *et al.* 2004) indicates that the necessary capacity is achievable given the form factor of the embedded sensor (which restricts the size of the piezoelectric wafer), the predicted usage scenario, the required charging time, and the low frequency vibrations of the structure.

4. Future work

4.1. System-level design and implementation

Completion of the project requires solutions to several system-level issues. We are currently designing wireless network configurations and system protocols that minimize the amount of time the modules must be fully powered. Additionally, we are implementing a suitable low-power microcontroller with adequate memory that will control both the sensing and communication aspects of module operation. This will be coupled with piezoelectric energy scavenging circuitry to power the embedded sensors over the useful lifetime of the structure. We anticipate that local bridge base stations will be designed to blend in to the aesthetics of the structure and will be powered using widely available rechargeable solar technology.

4.2. Accelerated corrosion tests and transducer configuration

To evaluate the ability of the proposed system to evaluate/characterize corrosion damage, accelerated corrosion tests are currently being conducted. Prior to accelerated corrosion, each specimen has been cured for twenty-eight days and immersed in a 5% NaCl bath for an additional three days to ensure uniform moisture distribution. Then, a copper mesh is used as the cathode and the reinforcing tendon is used as the anode for the reaction. The voltage and current are continuously monitored to estimate the percentage of corrosion using Faraday's Law. The percentage of corrosion estimated in this way has been confirmed by actual measurements of the mass loss of the steel reinforcement after being removed from the surrounding concrete. To further develop the proposed sensing system, ultrasonic transducers will also be mounted orthogonal to the tendon (indirect transducer configuration) on a long continuous beam. Accelerated corrosion will again be induced at certain locations along the beam to confirm the effectiveness of the proposed system to remotely detect/characterize corrosion damage.

5. Conclusions

This work describes ongoing development of an embedded sensor system for the early detection and prevention of deterioration of the reinforcing steel tendons within concrete bridge girders. These devices will evaluate the condition of the steel tendon using ultrasonic techniques and then wirelessly transmit this data to the outside world without human intervention. To maintain the structural integrity

of the reinforced concrete, these wireless embedded sensors are designed to present minimal volumes and their housing is designed to mimic the concrete stiffness to reduce stress concentrations. The complete sensor will be modest in size and a simple implementation procedure for installation in the girder mold will insure that no air voids are created. All electronics, including the antenna, will be sealed to prevent any corrosion or contamination. Both the antenna and communication link budget have been developed broadly enough to encompass changes in the conductivity of the concrete over time and with changes in the seasons.

The work outlined here shows the feasibility of both the detection of tendon conditions as well as the wireless link that will enable communication of this data to the outside world. Using commercially available off-the-shelf components, implementation of these devices has the potential to save millions of dollars a year in evaluation, repair and replacement of reinforced concrete girders.

Acknowledgments

References

Ansoft Corporation, HFSS$^©$, Version 9.1.

Auld, B. A. (1973), *Acoustic Fields and Waves in Solids: Volume II*, John Wiley & Sons, New York.

Carino, N. J. (1999), "Nondestructive techniques to investigate corrosion status in concrete structures", *J. Performance of Constructed Facilities*, **13**(3), 96-106.

Carkhuff, B. and Cain, R. (2003), "Corrosion sensors for concrete bridges", *IEEE Instrumentation & Measurements Magazine*, June 2003, 19-24.

Chung, H. W. (1978), "Effects of embedded steel bars upon ultrasonic testing of concrete", *Magazine of Concrete Research*, **30**(102), 19-25.

Fuhr, P. L. and Huston, D. (1998), "Corrosion detection in reinforced concrete roadways and bridges via embedded fiber optic sensors", *Smart Mater. Struct.*, **7**, 217-228.

Fuhr, T. P., Ambrose, T. P., Huston, D. R. and McPadden, A. J. (1995), "Fiber optic corrosion sensing for bridges and roadway surfaces", *Proceedings of the Smart Systems for Bridges, Structures, and Highways Conference*, **2446**, San Diego, CA.

Griffiths, J. (1987), *Radio Wave Propagation and Antennas*, Prentice-Hall International, Englewood Cliffs, New Jersey.

Howell, J. Q. (1975), "Microstrip antennas", *IEEE Transactions on Antennas and Propagation*, **23**(1), 90-93.

Huynh, T. and Lee, K. F. (1995), "Single-layer single-patch wideband microstrip antenna", *Electronics Letters*, **31**(16), 1310-1312.

Kolsky, H. (1963), *Stress Waves in Solids*, Dover Publications, Inc., New York.

Na, W., Kundu, T. and Ehsani, M. R. (2002), "Ultrasonic guided waves for steel bar concrete interface testing", *Materials Evaluation*, **60**(3), 437-444.

Ottman, G. K., Hofmann, H. F., Bhatt, A. C. and Lesieutre, G. A. (2002), "Adaptive piezoelectric energy harvesting circuit for wireless remote power supply", *IEEE Transactions on Power Electronics*, **17**(3), 669-676.

Ottman, G. K., Hofman, H. F. and Lesieutre, G. A. (2003), "Optimized piezoelectric energy harvesting circuit using step-down converter in discontinuous conduction mode", *IEEE Transactions on Power Electronics*, **18**(2), 696-703.

Pavlakovic, B. and Lowe, M. J. S. (2001), "Disperse User's Manual Version 2.0.11", Imperial College,

University of London.

Pavlakovic, B., Lowe, M. J. S. and Cawley, P. (1999) "The inspection of tendons in post-tensioned concrete using guided ultrasonic waves", *INSIGHT*, **41**(7), 446-452.

Ramo, S., Whinnery, J. R. and Van Duzer, T. (1994), *Fields and Waves in Communication Electronics*, 3rd Ed., John Wiley & Sons, Inc., New York.

Redwood, M. (1960), *Mechanical Waveguides*, Pergamon Press Ltd., New York.

Reis, H. L. M and Ervin, B. (2003), "Detection of corrosion in reinforced concrete structures using an ultrasonic approach", Technical Report UIUC ENG 03-3001, University of Illinois at Urbana-Champaign, Urbana, Illinois, 2003.

Rhim, H. C. and Büyüköztürk, O. (1998), "Electromagnetic properties of concrete at microwave frequency range", *ACI Mater. J.*, **95**(3), 262-271.

Rhim, H. C. and Büyüköztürk, O. (2000), "Wideband microwave imaging of concrete for nondestructive testing", *J. Struct. Eng.*, **126**(12), 1451-1457.

Rose, J. L. (1999), *Ultrasonic Waves in Solid Media*, University Press, Cambridge.

Rose, J. L. (2002), "A baseline and vision of ultrasonic guided wave inspection potential", *J. Pressure Vessel Technology*, **124**, 273-282.

Ross, R. and Goldstein, M. (2003), "Monitor warns of bridge corrosion", *Better Roads: Better Bridges*, August.

Sadano, H. A., Park, G., Leo, D. J. and Inman, D. J. (2003), "Use of piezoelectric energy harvesting devices for charging batteries", *Proc. SPIE 10th Annual International Symposium on Smart Structures and Materials*, 2-6 March, San Diego, CA.

Sadano, H. A., Park, G. and Inman, D. J. (2004), "Estimation of electric charge output for piezoelectric energy harvesting", *Strain*, **40**, 49-58.

Sinha, S. K., Schokker, A. J. and Shivprakash, R. I. (2003), "Non-contact ultrasonic imaging of post-tensioned bridges to investigate corrosion and void status", *Proceedings of 2003 IEEE Sensors*, 487-492.

Turner, C. W., Arif, M. Z. and Xia, X. (1994), "Characterization of concrete structures by acoustic resonance spectroscopy", *IEEE Ultrasonics Symposium*, 1107-1110.

Wang, C. S., Wu, F. and Chang, F- K. (2001) "Structural heath monitoring from fiber-reinforced composites to steel-reinforced concrete," *Smart Mater. Struct.*, **10**, 548-552.

Watters, D. G., Jayaweera, P., Bahr, A. J. and Huestis, D. L. (2002), "Design and performance of wireless sensors for structural health monitoring", *AIP Conference Proceedings*, May.

Weigand, S., Huff, G. H., Pan, K. and Bernhard, J. T. (2003), "Analysis and design of broadband single-layer rectangular u-slot microstrip patch antennas", *IEEE Transactions on Antennas and Propagation*, **51**(3), 457-468.

Wu, F. and Chang, F.-K., (2001) "A built-in active sensing diagnostic system for civil infrastructure systems, smart structures and materials", 2001: *Smart Systems for Bridges, Structures, and Highways*, S. C. Liu, Editor, *Proceedings of SPIE*, **4330**, 27-35.

Zeland Software, (1999), IE3D©, Version 8.0.

CC